Satellite measurements of the clear-sky greenhouse effect from tropospheric ozone

HELEN M. WORDEN[†][*], KEVIN W. BOWMAN[*], JOHN R. WORDEN, ANNMARIE ELDERING AND REINHARD BEER

Science Division, Jet Propulsion Laboratory, California Institute of Technology, 4800 Oak Grove Drive, Pasadena, California 91109, USA
[†]Present Address: Atmospheric Chemistry Division, National Center for Atmospheric Research, PO Box 3000, Boulder, Colorado 80307, USA
[*]e-mail: hmw@ucar.edu; Kevin.Bowman@jpl.nasa.gov

Radiative forcing from anthropogenic ozone in the troposphere is an important factor in climate change[1], with an average value of $0.35\,W\,m^{-2}$ according to the Intergovernmental Panel for Climate Change[1] (IPCC). IPCC model results range from 0.25 to $0.65\,W\,m^{-2}$, owing to uncertainties in the estimates of pre-industrial concentrations of tropospheric ozone[1–3], and in the present spatial and temporal distributions of tropospheric ozone[4–8], which are much more variable than those of longer-lived greenhouse gases such as carbon dioxide. Here, we analyse spectrally resolved measurements of infrared radiance from the Tropospheric Emission Spectrometer[9] on board the NASA Aura satellite, as well as corresponding estimates of atmospheric ozone and water vapour, to obtain the reduction in clear-sky outgoing long-wave radiation due to ozone in the upper troposphere over the oceans. Accounting for sea surface temperature, we calculate an average reduction in clear-sky outgoing long-wave radiation for the year 2006 of $0.48 \pm 0.14\,W\,m^{-2}$ between 45° S and 45° N. This estimate of the clear-sky greenhouse effect from tropospheric ozone provides a critical observational constraint for ozone radiative forcing used in climate model predictions.

The Tropospheric Emission Spectrometer (TES) is an infrared Fourier-transform spectrometer on board the NASA (National Aeronautics and Space Administration) Earth Observing System Aura platform[10]. Launched in July, 2004, Aura is in a near-polar, sun-synchronous orbit with equator crossing times of 13:40 and 2:29 local mean solar time for ascending and descending orbit paths, respectively. TES is predominantly nadir viewing and measures radiance spectra at frequencies between 650 and $2{,}250\,cm^{-1}$ of the Earth's surface and atmosphere. TES was designed with sufficiently fine spectral resolution ($0.06\,cm^{-1}$, unapodized) to measure the pressure-broadened infrared absorption lines of ozone in the troposphere[9]. Along with ozone profiles, atmospheric temperature, concentrations of water vapour, deuterated water vapour, carbon monoxide and methane, effective cloud pressure and optical depth, surface temperature and land emissivity are derived from TES radiance spectra. The TES forward model[11] used for computing spectral radiances in atmospheric retrievals is based on a line-by-line radiative transfer model, which has been used extensively for calculating atmospheric heating and cooling rates[12]. Radiometric calibration, retrieval algorithms and error characterization have been described previously[13–16].

TES radiances have been validated using the Atmospheric Infrared Sounder (AIRS) spectrometer on Aqua, which is ∼15 min ahead of Aura. For the ozone absorption band near $9.6\,\mu m$, TES V002 data have a 0.12 K cold bias with respect to AIRS (ref. 17), which is within the accuracy of AIRS radiance measurements, 0.2 K (ref. 18). TES ozone retrievals have been compared with ozonesondes[19] and have a consistent high bias, ∼10 p.p.b. in the troposphere, which is accounted for in this analysis. The vertical resolution for ozone profiles is 6–7 km, and vertical sensitivity, as quantified by degrees of freedom[13], is ∼1.5 degrees of freedom in the troposphere for clear-sky tropics and subtropics[20].

Unlike water vapour, the bulk of ozone absorption in the infrared region is confined to the spectral range around $9.6\,\mu m$. To compute the top-of-atmosphere (TOA) flux associated with infrared ozone absorption, TES radiance spectra are integrated and converted to flux in $W\,m^{-2}$ (see the Methods section). To remove the largest sources of variability in nadir radiance spectra (clouds and land), we select clear-sky ocean scenes (see Supplementary Information, Fig. S1) using TES spectra and atmospheric retrievals with corresponding cloud[14] effective optical depth <0.05. For clear-sky tropical (30° S to 30° N) ocean scenes, Huang *et al.*[21] compute an average flux of $18\,W\,m^{-2}$ from 1970 Infrared Interferometer Spectrometer (IRIS) spectra for the 985–$1{,}080\,cm^{-1}$ ozone band. Over the same latitudes and frequency range used with the IRIS spectra, we obtain $18.6 \pm 0.15\,W\,m^{-2}$ (uncertainty from radiometric accuracy and anisotropy assumptions) with a standard deviation of $0.8\,W\,m^{-2}$ for the annual average (December 2005 to November 2006) clear-sky, ocean flux from TES spectra, consistent with the IRIS data.

Previous studies have used satellite radiance spectra to demonstrate decadal greenhouse gas changes[22] and to test whether general circulation and climate model predictions reproduce the sources of variability present in the spectra[23,24]. These studies have shown how spectral resolution enables characterization of the parameters that drive outgoing long-wave radiation (OLR) variability beyond what can be obtained with broadband OLR measurements such as those from the Clouds and the Earth's

305
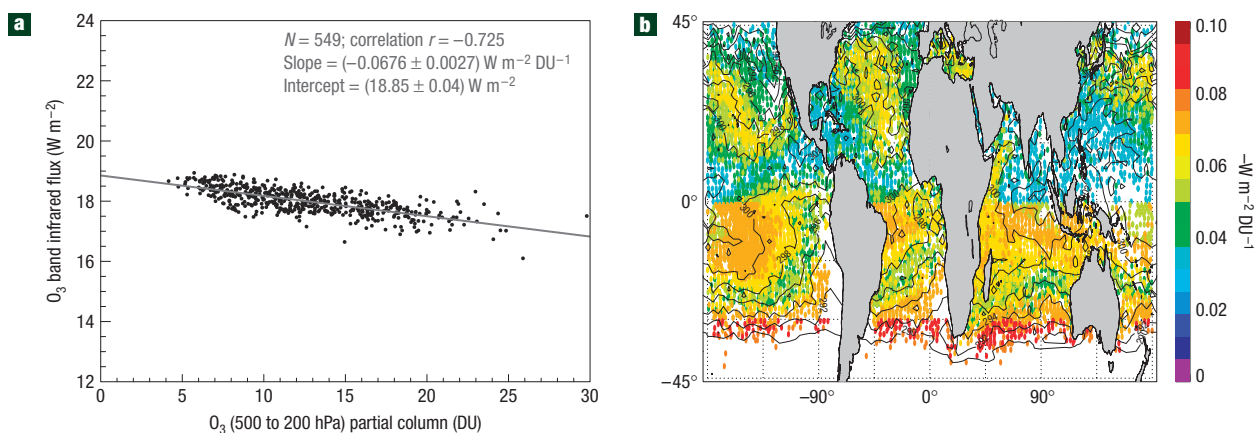
Figure 1 TES ensemble sensitivities of TOA infrared flux to upper tropospheric ozone. a, Example of linear fit of TOA infrared flux to upper tropospheric ozone (partial column ozone from 500 to 200 hPa). The case shown is for JJA 2006 northern hemisphere SSTs between 298 and 299 K. **b**, Map of JJA 2006 ensemble sensitivities in negative $W m^{-2} DU^{-1}$. 2 K SST contours are overplotted to show the spatial dependence on SST binning.

Radiant Energy System (CERES) or the Earth Radiation Budget Experiment (ERBE)[25]. Following an approach similar to that of Huang *et al.*[24], but focusing on the infrared ozone band and examining only clear-sky ocean observations, we determine the primary contributions to the variability in the TOA flux through decomposition of TES spectra into orthogonal principal component vectors (see the Methods section and Supplementary Information). On the basis of the correlations of retrieved atmospheric and surface parameters to the projections of the measured spectra onto the principal components (expansion coefficients, equation (1) in the Methods section), we find that the variability of the TOA ozone band flux in the tropics is explained primarily by sea surface temperature (SST) followed by tropospheric water vapour and upper tropospheric ozone (see Supplementary Information, Figs S3–S5). Here, we define tropospheric water vapour as the average volume mixing ratio between the surface and 200 hPa, and upper tropospheric ozone as a partial column (in DU) between 500 and 200 hPa. Note that only TES profiles where the tropopause pressure was less than 200 hPa were used in this analysis, which is necessary when considering latitudes from 45° S to 45° N using a consistent definition of upper tropospheric column. This principal component analysis demonstrates that SST must be fixed to determine sensitivities of the TOA ozone band flux to both ozone and water vapour.

Accounting for SST dependence by binning the data as a function of SST (see the Methods section), we compute ensemble clear-sky OLR (OLRc) sensitivities as the linear slopes of flux versus upper tropospheric ozone in $W m^{-2} DU^{-1}$ and versus tropospheric water in $W m^{-2}$ per volume mixing ratio for each SST bin. Figure 1a shows an example of a linear fit to flux versus ozone with the slope representing the ensemble OLRc sensitivity for a specific SST range. The slope computed for each SST bin was always negative and significantly different from zero, with >99% confidence level assuming gaussian errors from the fit, except for northern hemisphere SST bins from 301 to 302 K and 302 to 303 K for March/April/May (MAM). These MAM, high SST slopes are also negative but different from zero with a 93% and 81% confidence level, respectively; they do not affect the significance when considering annual average values. Results of the ensemble sensitivities to water vapour and upper tropospheric ozone as a function of season, hemisphere and SST are shown in Supplementary Information, Fig. S6. Figure 1b shows the map of

ensemble OLRc sensitivities for June/July/August (JJA) 2006. The spatial morphology is determined by SST patterns and the arbitrary northern/southern hemisphere split in our binning.

The TES 2006 annual average for ensemble OLRc sensitivity to upper tropospheric ozone is $0.055 W m^{-2} DU^{-1}$ with a standard deviation of 0.017 (for 45° S to 45° N). Gauss *et al.*[4] give a range of $0.042–0.052 W m^{-2} DU^{-1}$ for the global annual averages from 11 different climate model estimates of long-wave, clear-sky normalized radiative forcing for tropospheric ozone over the 21st century. Note that the TES average excludes higher latitudes where model estimates of normalized forcing are lower. Whereas the models tend to show the highest sensitivities in the subtropics[4], TES values are generally higher for mid-latitudes. As ozone near the tropopause will have the largest radiative forcing[5], we should expect this type of latitude dependence in the OLRc sensitivity based on our definition of upper tropospheric column, 500–200 hPa, which will be closer to the tropopause at higher latitudes. Both observations and models show a lower sensitivity to tropospheric ozone over the Indian Ocean and the Pacific warm pool.

By multiplying the ensemble flux sensitivities with the corresponding distributions of TES partial columns for the upper troposphere, we create a map of the reduced OLRc due to upper tropospheric ozone between 500 and 200 hPa for cloud-free ocean conditions. Figure 2 shows the resulting OLRc reduction values for December 2005 to November 2006 with averages mapped in 1° latitude, 1° longitude bins. The annual average value for 45° S to 45° N is $0.48 \pm 0.14 W m^{-2}$. TES tropospheric ozone values were lowered by 15% to account for the known high bias of TES compared with ozonesondes[19]. To compute the measurement uncertainty, $\pm 0.14 W m^{-2}$, the following independent errors, in order of dominance, are added in quadrature: anisotropy uncertainty ($\pm 0.13 W m^{-2}$), total retrieval error for the 500–200 hPa partial ozone column (1.1 DU), which includes contamination from the lower troposphere and stratosphere associated with TES vertical resolution, uncertainty of the TES ozone bias with ozonesondes over the latitudes considered ($\pm 5\%$) and the mean slope error from the SST bin linear fits ($\pm 1.2\%$).

Figure 2 shows that the reduced OLRc from upper tropospheric ozone is highly variable on a global scale. For the TES-estimated annual average OLRc reduction of $0.48 W m^{-2}$, the corresponding standard deviation, $0.24 W m^{-2}$, is mainly due to the large
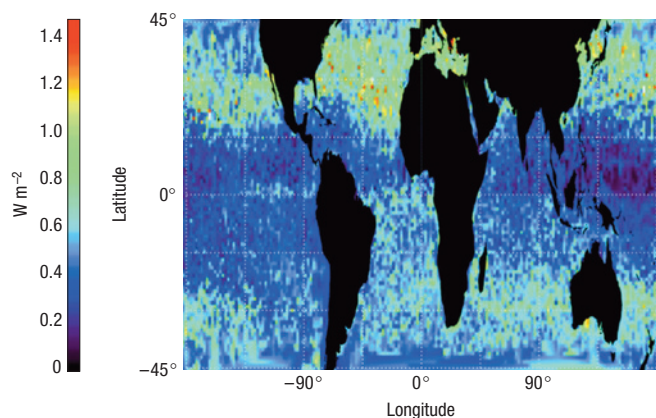
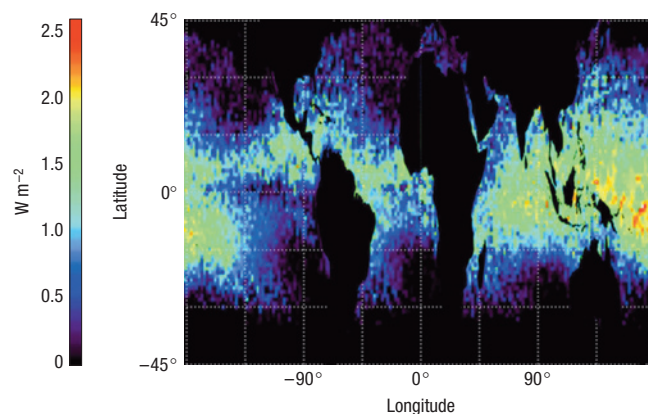**Figure 2 Annual average OLRc reduction from upper tropospheric ozone in W m⁻².** Upper tropospheric ozone is measured by the partial column (DU) from 500 to 200 hPa. Averages are mapped in 1° latitude, 1° longitude bins and include cloud-free ocean TES observations from December 2005 to November 2006. Measurement uncertainties correspond to ~1 colour bar gradation.

Figure 3 Annual average flux reduction in 9.6 μm ozone band from tropospheric water vapour. Tropospheric water vapour is measured as the average volume mixing ratio from the surface to 200 hPa. Averages are mapped in 1° latitude, 1° longitude bins and include cloud-free ocean TES observations from December 2005 to November 2006. Sensitivity to water vapour is only significant for SST > 295 K. Dark regions at mid-latitudes indicate where water vapour does not have a significant contribution to ozone band flux reduction.

variability of upper tropospheric ozone. The average ozone column from 500 to 200 hPa is 8.6 DU for the observations used in this analysis, with a standard deviation of 3.0 DU. Seasonal maps of OLRc reduction from upper tropospheric ozone exhibit significant temporal variability (see Supplementary Information, Fig. S7). The largest OLRc reduction values (up to 1.4 W m⁻²) are observed for spring in the northern hemisphere, and can be associated with the tropospheric ozone spring-time maximum[26]. In austral winter, ozone from biomass burning[27] also has a large impact, ~0.9 W m⁻².

OLRc sensitivity to lower tropospheric ozone was also investigated. On the basis of our principal component correlation analysis (see the Methods section), we found that radiance variability is much less sensitive to these distributions over ocean. However, we note that sensitivity to the lower troposphere, along with diurnal variations can be significant when estimating OLR reduction from tropospheric ozone over land.

Although we compute the ensemble sensitivities to tropospheric water vapour for the TOA flux from 985–1,080 cm⁻¹ in all SST bands, they are significant compared with those for ozone only for SST bins higher than 295 K. At SSTs higher than 299 K, the variability and OLRc reduction due to water vapour is larger than that due to ozone. Figure 3 shows the annual average OLRc reduction in the infrared ozone band due to tropospheric water vapour for December 2005–November 2006. Plots for each season of OLRc reduction due to water vapour are shown in Supplementary Information, Fig. S8. The dominance of the water vapour contribution in the ozone band for the higher SST bins is consistent with the 'super' greenhouse gas effect[28,29], where water vapour feedback causes a higher rate of total greenhouse forcing with respect to SST.

The 2007 Intergovernmental Panel for Climate Change average radiative forcing for tropospheric ozone is defined as the net downward flux, including the smaller short-wave contribution, at the tropopause due to the anthropogenic increase in tropospheric ozone from pre-industrial times and is based purely on model simulations[1]. Both natural and anthropogenic ozone contribute to the instantaneous radiative forcing, or OLR reduction, from ozone, which we show can be estimated from satellite measurements. The reduced OLRc from upper tropospheric ozone presented here is an important observational constraint for climate models, which must accurately reproduce the effects on OLRc from both anthropogenic and natural forcings. Ozone enhancements from increasing emissions will amplify climate change through both direct and indirect radiative effects, with implications for both global and regional hydrological cycles[1,30]. Consequently, satellite measurements that can differentiate sources of variability in the outgoing flux, such as ozone and water vapour, represent critical climate observables.

METHODS

To convert TES spectral radiances in W/cm²/sr/cm⁻¹ to ozone band flux values in W m⁻², we integrate over frequency from 985 to 1,080 cm⁻¹ and carry out the angular integration assuming the long-wave anisotropy factor $R(\theta)$ varies smoothly with off-nadir angle[25] and has the value $R = 1.05$ for TES nadir views ($\theta = 0$). This anisotropy factor is the average of tabulated angular distribution models for the Clouds and the Earth's Radiant Energy System[25] 8–12 μm window band, clear-sky ocean nadir views, with a 0.7% standard deviation, accounting for variations in anisotropy due to the range of temperature and humidity conditions. We note that this value underestimates the anisotropy for the ozone band, which is a spectral subset of the 8–12 μm window band. The anisotropy for the window band is an average of lower anisotropy values (close to 1 for ocean scenes) corresponding to lower atmospheric absorption and higher values for the spectral range with ozone absorption. The resulting high bias in flux or flux sensitivity calculations (<10%) will be addressed in future work with more accurate anisotropy estimates. The conversion factor for frequency-integrated radiance to flux is then 10,000 (cm² m⁻²)πsr/1.05. The contribution of instrument noise to the total error after integration is negligible, ~0.00003 W m⁻², on the basis of a noise-equivalent spectral radiance ~38 nW/cm²/sr/ cm⁻¹ for each of the 1,533 spectral points. TES radiometric accuracy is ~0.07 W m⁻² for TOA flux, but, as a systematic error, will cancel in the slope from a linear fit to flux values.

We use singular value decomposition to determine the principal components of variability in clear-sky ocean TES spectra from 985 to 1,080 cm⁻¹. The weighted contributions of the leading singular vectors to the spectral radiances for each observation were calculated and spectrally integrated to yield the following expansion coefficients:

$$\mathrm{EC}_i(x) = \int_\nu [\alpha_i(x)\phi_\nu^{(i)} + \overline{I_\nu}]\,\mathrm{d}\nu, \qquad (1)$$

where ν is the frequency, $\overline{I_\nu}$ is the mean spectrum over all observations, $\phi_\nu^{(i)}$ is the ith spectral singular vector and $\alpha_i(x) = \langle[I_\nu(x) - \overline{I_\nu}], \phi_\nu^{(i)}\rangle$ is the

projection of a mean-subtracted spectrum at location x onto the ith spectral singular vector. The expansion coefficients (converted to flux in W m^{-2}) can be related to physical parameters estimated from each TES observation. For the tropics from 15° S to 15° N, JJA, 2006, the first three singular vectors for the mean-subtracted spectra account for 94% of the observed variability (see Supplementary Information, Fig. S2). The spatial distributions of the expansion coefficients were correlated with the distributions of SST, tropospheric water vapour and lower tropospheric, upper tropospheric and stratospheric ozone (see Supplementary Information, Figs S3–S5). The first expansion coefficient, EC_1, correlated best with SST ($r = 0.59$), whereas EC_2 had the highest correlations with water vapour and SST ($r = -0.68$ and -0.67 respectively). EC_3 had the highest correlation with upper tropospheric ozone ($r = -0.6$).

To account for SST dependence, we compute OLRc sensitivities to ozone using linear fits of flux versus upper tropospheric ozone partial column for ensemble data sets binned by SST. A total of 39,302 TES nadir observations over four seasons, December/January/February, MAM, JJA and September/October/November, were separated into northern and southern hemispheres and binned into sea surface temperatures with 2 K bins between 286 to 294 K and 1 K bins for SSTs between 294 and 304 K. Ensemble sets with less than 100 data points per bin were not used, leaving some blank regions at higher latitudes, especially in the northern hemisphere where there are comparatively fewer cloud-free ocean scenes. A separate singular value decomposition was computed for the spectral data in each SST bin. Expansion coefficients (EC_1 and EC_2) corresponding to the leading spectral singular vectors for each ensemble had the highest correlations ($r \sim 0.6$–0.8) with either upper tropospheric O_3 or tropospheric water vapour. Correlations of EC_1 and EC_2 with other ozone subcolumns, such as stratospheric ozone (100 to 0.1 hPa) or lower tropospheric ozone (surface to 500 hPa), were always smaller ($r \sim 0.4$ or lower). EC_1 had the highest correlations with upper tropospheric O_3 for mid-latitude SST bins, whereas EC_1 correlation with water vapour is dominant in the tropics, beginning at SSTs > 299 K.

Finally, we note that it would be possible to determine the sensitivity of OLRc to tropospheric ozone, explicitly accounting for SST and other retrieved parameters, if we could integrate the jacobians, that is, partial derivatives of TOA radiance with respect to log (volume mixing ratio) for ozone and water vapour on a vertical grid, computed by the forward model in the TES retrieval algorithm. However, jacobians are not stored for later analysis in operational TES data processing owing to prohibitive data storage requirements. In future studies, it may be possible to store jacobians, integrated over frequency ranges of interest, such as the 9.6 µm ozone band. This would enable the evaluation of OLR sensitivity to ozone, at any vertical level, over ocean and land, for both clear and cloudy conditions. This study represents motivation for such future work.

References
1. Forster, P. et al. in *The Fourth Assessment Report of the Intergovernmental Panel on Climate Change* (ed. Soloman, S. et al.) (Cambridge Univ. Press, Cambridge, 2007).
2. Gauss, M. et al. Radiative forcing since preindustrial times due to ozone change in the troposphere and the lower stratosphere. *Atmos. Chem. Phys.* **6**, 575–599 (2006).
3. Mickley, L. J., Jacob, D. J. & Rind, D. Uncertainty in preindustrial abundance of tropospheric ozone: Implications for radiative forcing calculations. *J. Geophys. Res. Atmos.* **106**, 3389–3399 (2001).
4. Gauss, M. et al. Radiative forcing in the 21st century due to ozone changes in the troposphere and the lower stratosphere. *J. Geophys. Res. Atmos.* **108**, 4292–4313 (2003).
5. Kiehl, J. T. et al. Climate forcing due to tropospheric and stratospheric ozone. *J. Geophys. Res. Atmos.* **104**, 31239–31254 (1999).
6. Naik, N. et al. Net radiative forcing due to changes in regional emissions of tropospheric ozone precursors. *J. Geophys. Res. Atmos.* **110**, D24306 (2005).
7. Portmann, R. W. et al. Radiative forcing of the Earth's climate system due to tropical tropospheric ozone production. *J. Geophys. Res. Atmos.* **102**, 9409–9417 (1997).
8. Stevenson, D. S. et al. Multimodel ensemble simulations of present-day and near-future tropospheric ozone. *J. Geophys. Res. Atmos.* **111**, D08301 (2006).
9. Beer, R. TES on the Aura mission: Scientific objectives, measurements, and analysis overview. *IEEE Trans. Geosci. Remote Sens.* **44**, 1102–1105 (2006).
10. Schoeberl, M. R. et al. Overview of the EOS Aura mission. *IEEE Trans. Geosci. Remote Sens.* **44**, 1066–1074 (2006).
11. Clough, S. A. et al. Forward model and Jacobians for tropospheric emission spectrometer retrievals. *IEEE Trans. Geosci. Remote Sens.* **44**, 1308–1323 (2006).
12. Clough, S. A. & Iacono, M. J. Line-by-line calculation of atmospheric fluxes and cooling rates 2. Application to carbon dioxide, ozone, methane, nitrous oxide and the halocarbons. *J. Geophys. Res. Atmos.* **100**, 16519–16535 (1995).
13. Bowman, K. W. et al. Tropospheric emission spectrometer: Retrieval method and error analysis. *IEEE Trans. Geosci. Remote Sens.* **44**, 1297–1307 (2006).
14. Kulawik, S. S. et al. Implementation of cloud retrievals for Tropospheric Emission Spectrometer (TES) atmospheric retrievals: Part 1. *J. Geophys. Res. Atmos.* **111**, D24204 (2006).
15. Worden, H. M. et al. TES level 1 algorithms: Interferogram processing, geolocation, radiometric, and spectral calibration. *IEEE Trans. Geosci. Remote Sens.* **44**, 1288–1296 (2006).
16. Worden, J. et al. Predicted errors of tropospheric emission spectrometer nadir retrievals from spectral window selection. *J. Geophys. Res. Atmos.* **109**, D09308 (2004).
17. Shephard, M. W. et al. Tropospheric emission spectrometer spectral radiance comparisons. *J. Geophys. Res. Atmos.* (in the press).
18. Tobin, D. C. et al. Radiometric and spectral validation of atmospheric infrared sounder observations with the aircraft-based scanning high-resolution interferometer sounder. *J. Geophys. Res. Atmos.* **111**, D09S02 (2006).
19. Nassar, R. et al. Validation of tropospheric emission spectrometer (TES) nadir ozone profiles using ozonesonde measurements. *J. Geophys. Res. Atmos.* (in the press).
20. Jourdain, L. et al. Tropospheric vertical distribution of tropical Atlantic ozone observed by TES during the northern African biomass burning season. *Geophys. Res. Lett.* **34**, L04810 (2007).
21. Huang, X. L., Ramaswamy, V. & Schwarzkopf, M. D. Quantification of the source of errors in AM2 simulated tropical clear-sky outgoing longwave radiation. *J. Geophys. Res. Atmos.* **111**, D14107 (2006).
22. Harries, J. E., Brindley, H. E., Sagoo, P. J. & Bantges, R. J. Increases in greenhouse forcing inferred from the outgoing longwave radiation spectra of the Earth in 1970 and 1997. *Nature* **410**, 355–357 (2001).
23. Haskins, R. D., Goody, R. D. & Chen, L. A statistical method for testing a general circulation model with spectrally resolved radiances. *J. Geophys. Res. Atmos.* **102**, 16563–16581 (1997).
24. Huang, X. L. & Yung, Y. L. Spatial and spectral variability of the outgoing thermal IR spectra from AIRS: A case study of July 2003. *J. Geophys. Res. Atmos.* **110**, D12102 (2005).
25. Loeb, N. G. et al. Angular distribution models for top-of-atmosphere radiative flux estimation from the Clouds and the Earth's Radiant Energy System instrument on the Terra Satellite. Part I: Methodology. *J. Atmos. Oceanic Technol.* **22**, 338–351 (2005).
26. Oltmans, S. J. et al. Tropospheric ozone over the North Pacific from ozonesonde observations. *J. Geophys. Res. Atmos.* **109**, D15S01 (2004).
27. Fishman, J., Watson, C. E., Larsen, J. C. & Logan, J. A. Distribution of tropospheric ozone determined from satellite data. *J. Geophys. Res.* **95**, 3599–3617 (1990).
28. Raval, A. & Ramanathan, V. Observational determination of the greenhouse effect. *Nature* **342**, 758–761 (1989).
29. Valero, F. P. J., Collins, W. D., Pilewskie, P., Bucholtz, A. & Flatau, P. J. Direct radiometric observations of the water vapor greenhouse effect over the equatorial Pacific ocean. *Science* **275**, 1773–1776 (1997).
30. Sitch, S., Cox, P. M., Collins, W. J. & Huntingford, C. Indirect radiative forcing of climate change through ozone effects on the land-carbon sink. *Nature* **448**, 791–794 (2007).

Supplementary Information accompanies this paper on www.nature.com/naturegeoscience.

Author contributions
H.M.W. drafted the manuscript, prepared the figures and developed the methods for estimating OLRc sensitivity. K.W.B. drafted sections for the manuscript and methods, and provided tools and interpretation for the principal component analysis. J.R.W. provided error estimates and analysis tools. A.E. provided analysis tools and interpretation. R.B. developed the TES experiment and instrument. R.B. and A.E. are responsible for project planning. All authors contributed to discussions of the results and preparation of the manuscript.

Author information
Reprints and permission information is available online at http://npg.nature.com/reprintsandpermissions. Correspondence and requests for materials should be addressed to H.M.W. or K.W.B.